Electronic Supporting Information (ESI)

Strategic Catalyst Modification for Boosting CO_2 Concentration at Electrode Surface and Easing Selective CO_2 Reduction at Higher Potential

Shuvojit Mandal and Praveen Kumar*

School of Materials Science, Indian Association for the Cultivation of Science, Kolkata-700032, India

*Corresponding Author Email: praveen.kumar@iacs.res.in

Experimental Section:

Specifications of chemicals:

$BiCl_3$ (trace metal basis, 99.99%), $NaBH_4$ (>98%), 2-Ethoxyethanol, and DMSO (99.9%) are bought from Sigma Aldrich. $KHCO_3$, Ammonium persulfate, Formic acid (98-100%) Hydrazine hydrate solution (80%), Aniline, Liquor ammonia (25%), Isopropanol, Hydrochloric acid (37%) are bought from Merck. Toray Carbon paper (TGP-H-60, 19×19 cm) is bought from Alfa Aesar. All the chemicals and materials are used as received without further treatment. All the aqueous solutions are made with Merck water. Ultra-high pure, 99.999% CO_2 and N_2 are supplied by IRS.

Synthesis:

2D BiOCl synthesis: In a typical synthesis, 473 mg of $BiCl_3$ is added to 50 ml 2-Ethoxyethanol in a 250 ml round bottom flask and sonicated to dissolve completely. This mixture is then heated to 120 °C for 30 min with a reflux condenser in an N_2 environment. It is naturally cooled to room temperature and a 5 ml aqueous solution of 80 µl hydrazine hydrate, is very slowly added dropwise into it while stirring in an open atmosphere. The solution is further stirred for 5 minutes and bath sonicated for 30 minutes at room temperature. Finally, BiOCl flakes are collected by centrifuging at 10000 rpm for 5 minutes and washed several times with 2-ethoxy ethanol, DI-water and Isopropanol (IPA), respectively. The collected powder was dried and stored inside a vacuum desiccator.

2D Bi Flakes synthesis: 100 mg of as-prepared BiOCl was re-dispersed in IPA via bath sonication and 10 ml of aqueous solution of 100 mg $NaBH_4$ (excess) was slowly dropwise added with stirring. The initial white dispersion become black and after a few minutes of stirring lump mass was formed which is filtered. The mass was redispersed via sonication and washed with N_2-purged DI-water and IPA and consequent centrifugation several times. Finally, it was vacuum dried.

PANI synthesis: In an ice bath, 1 ml Aniline is dissolved in 50 ml H_2O with 4.16 ml (1 M solution) of HCl in a 100 ml beaker and stirred for 15 minutes to obtain a clear solution. Then, a separately prepared 50 ml aqueous solution of 2.509 g Ammonium persulphate (0.22 M solution) was dropwise added to the solution with continuous stirring. The colorless solution turns light green then dark green and after 6 h of stirring the PANI Salt is collected via centrifugation and washed with DI water, IPA and acetone several times and finally dried.

500 mg of as-prepared PANI salt powder was added in 50 ml aqueous solution of 3.73 ml liqueur Ammonia (1 M solution) for overnight with stirring. Then it was washed with DI water several times until pH reaches 7 and further, the violet solution was washed out with acetone. Finally, the obtained PANI Base is dried and stored in a vacuum desiccator.

P-Bi synthesis (PANI soaking of Bi flakes): 5 mg of PANI dissolved in 10 ml DMSO via sonication and stirred for 5 min. Then 10 mg of Bi flakes are added and stirred for 48 h and it was centrifuged at 10000 rpm for 5 min and washed cautiously with a minimal amount of DMSO and then with IPA and dried and collected as a P-Bi sample inside a vacuum desiccator.

Electrode preparation: All the electrodes are prepared on carbon fiber paper and catalyst ink is drop casted cautiously on both sides of a 0.5×1.5 cm^2 carbon strip with 0.5×1 cm^2 area so that considering both sides, the final active electrode surface area becomes 1 cm^2. All the samples are dispersed in 300 µl IPA without any binding agent like Nafion solution and sonicated for 20 minutes before drop casting. We have optimized mass loading of Bi by taking chronoamperometry at -1.04 V_{RHE} with 1 mg, 2 mg and 3 mg catalyst loading for 1 h. We found 2 mg catalyst loading gives highest formate partial current density. We kept catalyst loading fixed to 2mg also fixed geometrical surface area for P-Bi electrode to normalize the comparison between Bi and P-Bi.

Measurement technique:

X-ray diffraction (XRD) was performed on the Rigaku SmartLab X-ray diffractometer where Cu-Kα was the source. LabRAM HR Jovin Yvon (with 488 nm laser excitation to analyze below 100 cm^{-1} peaks) and Horiba T64000 (with 532 nm laser excitation) Raman spectrometer were used for Raman spectroscopy. Field emission gun scanning electron microscopy (FE-SEM) (JEOL JSM-7500F), Atomic Force Microscopy (AFM) (Asylum Research MFP-3D using AC160TS silicon probes) in tapping mode and field emission gun transmission electron microscopy (FEG-TEM) (JEOL, JEM 2100F) were used for the characterization of surface morphology, Particle height profile, elemental analysis and further AFM images are processed with WSxM 5.0 and TEM images with the help of Gatan DigitalMicrograph software. Dynamic Light Scattering (DLS) (Malvern Zetasizer S90 series) is used for particle size analysis. UV–VIS-NIR absorption spectra were obtained from CARY 60, Agilent technologies, and UV–VIS-NIR spectrophotometer. Omicron Nano-technology X-ray photoelectron spectroscopy (XPS) was used to analyze the oxidation state and surrounding electronic environment.

Electrochemical Measurement technique:

The performance of the electrodes is assessed via an electrochemical workstation (Bio-Logic Science Instruments, Model SP-300/240). LSV and CA are measured in three-electrode modes with Pt mesh as a counter electrode and Ag/AgCl as a reference electrode (CH Instruments) in a customized H-type cell. LSV presented in the main text, is obtained at 20 mV/s scan rate. CO_2 saturated 0.5 M $KHCO_3$ aqueous electrolyte with pH=7.4, is used for all the measurements. All potentials are reported here with respect to Reversible Hydrogen Electrode (RHE) is converted via the following equation –

$$E\ (vs\ RHE) = E\ (vs\ Ag/AgCl) + 0.222\ V + 0.059\ V \times pH$$

After 1h Chrono amperometry at a particular potential, we analyzed the gas product with a GC analyzer (TRACE 1110, Thermo Scientific) and the Liquid product in 400 MHz NMR (Bruker Avance DPX 400 MHz spectrometer). We have prepared NMR locking standard by adding 2 µl of DMSO as an internal standard in 1ml D_2O (for NMR locking). And obtaining the standardization curve (**Figure S9b**), we added 0.5 ml of aqueous solution with a known amount of 99.9% formic acid and 0.1 ml of NMR locking standard. In a typical NMR sample preparation, we have taken 0.5 ml of electrolyte solution with 0.1 ml of already prepared locking standard. Form ^1H NMR, in water suppression mode, we can quantitively estimate formate formation from

the ratio of area under peak calculation with the help of a standardization curve. Finally, formate FE is calculated by the below equation –

$$FE_{Formate}(\%) = \frac{Q_{Formate}}{Q_{total}} \times 100\% = \frac{n_{Formate} \times N \times F}{j \times t} \times 100\%$$

Where, $n_{formate}$ is the amount of formate produced, N is the number of electrons transferred (2 for formate), and F is the Faradaic constant.

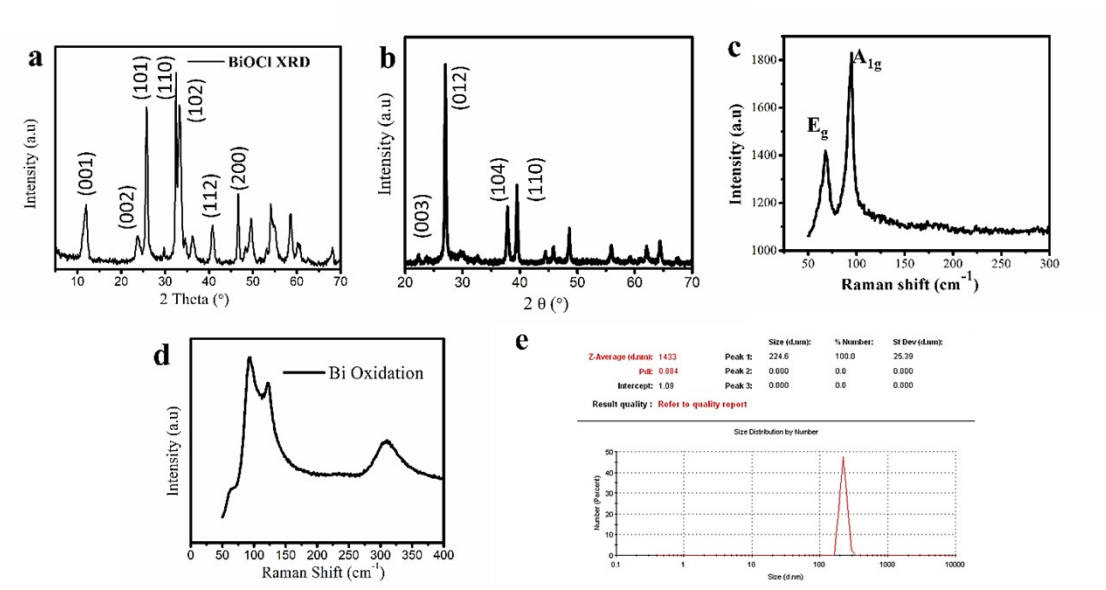

Figure S1: a) XRD of BiOCl, b) XRD of Bi flakes, c) Raman spectra of Bi flakes, d) laser-induced Bi flakes oxidation, e) DLS particle size analysis

Supplementary Note for Figure S1:

XRD data of a) BiOCl[1] and b) Bi flakes[2] signify successful synthesis. Raman data[3,4] are also consistent.

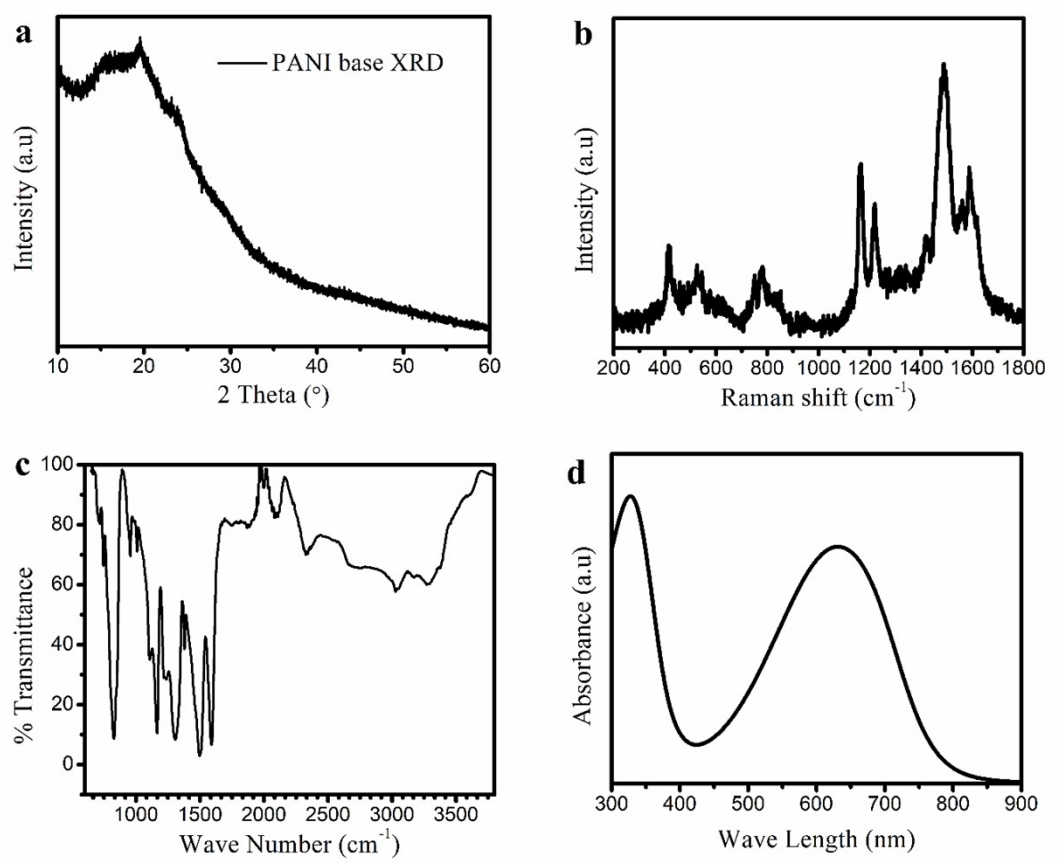

Figure S2: a) XRD of PANI base, b) Raman of PANI, c) FT-IR of PANI d) UV-Vis of PANI

Supplementary Note for Figure S2:

XRD data of the PANI base is showing a mostly amorphous nature with minor peaks at 15.5, 19.7 and 23.5°.[5] FT-IR spectra showing peaks at 826 (para substitution in the ring), 956 (out of plane C-H bending) 1009, 1110,1167 (are related to in-plane bending of aromatic C-H), 1307 (C-N stretching), 1500 (C=C stretching in quinonoid form), 1590 (C=C stretching of the benzenoid form) 3034 (C-H stretching vibration) 3285 (N-H stretching vibration) cm^{-1}. This suggests a successful synthesis of PANI.[6] Raman scattering shows peaks at 532 (Out of plane torsion/C-N-C), 778 (C-H out-of-plane bending vibration) 1162 (C-H in-plane-bending vibration of benzenoid ring), 1219 (C-N stretching mode), 1488 (C=N stretching mode of quinonoid form), 1588 (C=C stretching vibration of quinonoid form) cm^{-1}.[5,7,8] Again this Raman data supports the conclusion drawn from FT-IR data. UV-Vis spectra show an absorption band at 630 nm with another peak at the UV region, signifying proper neutralization of PANI salt and the presence of only pure PANI base.[9]

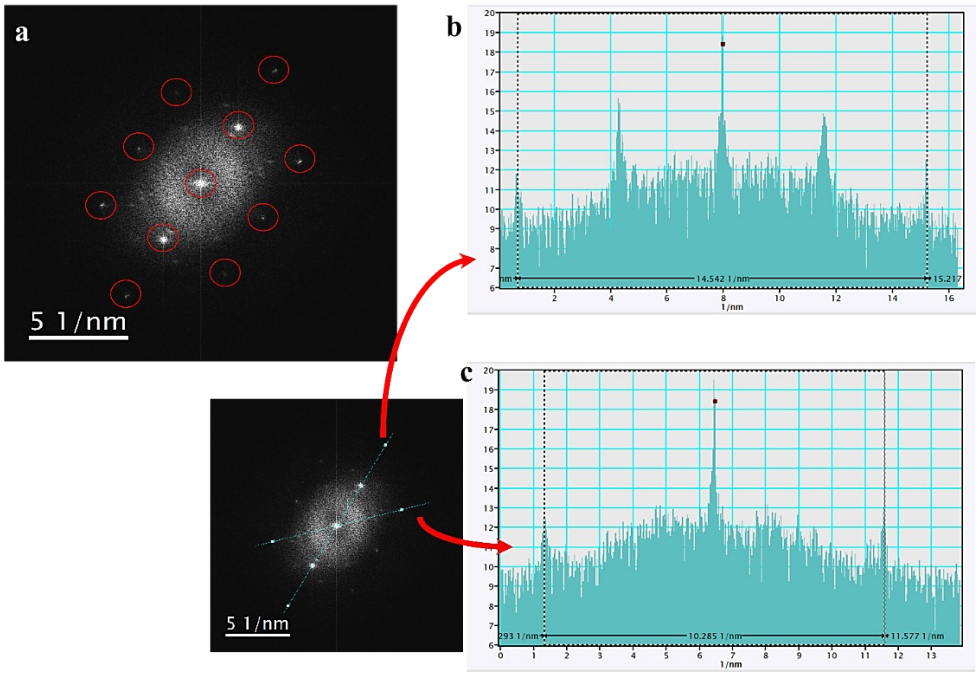

Figure S3: BiOCl HR-TEM and FFT analysis

Supplementary Note for Figure S3:

The a) FFT image spots are highlighted with a red circle showing a cubic lattice of BiOCl. The line scan along the middle of the cube is shown in Figure S3 b, showing $4\times(1/d_{hkl}) = 14.542$ nm^{-1} and the line scan along the corner in S3 c, showing $2\times(1/d_{hkl}) = 10.285$ nm^{-1}

Now, from Bragg's law, $2d_{hkl}Sin\theta = n\lambda$ and putting n=1 and λ=0.154 nm, we found corresponding 2θ=32.5° and 46.6°. The XRD peak at 32.5° is the most intense peak as shown in Figure S1 a corresponds to the (110) facet.

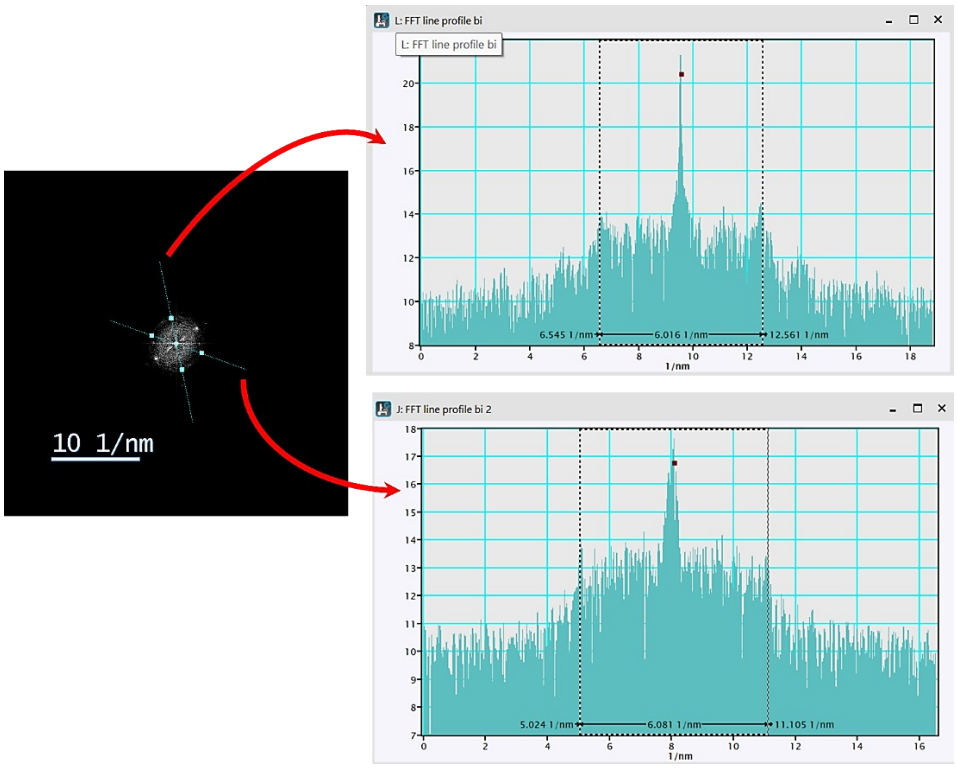

Figure S4: FFT analysis of Bi flake

Supplementary Note for Figure S4:

In the hexagonal FFT image, we have taken two line scans, showing $2\times(1/d_{hkl}) = (6.016+6.081)/2$ $nm^{-1} = 6.0485$ nm^{-1} (average is taken because of hexagonal packing and both the distance are not same because of minute errors).

Again, from Bragg's law, $2d_{hkl}Sin\theta = n\lambda$ and putting $n=1$ and $\lambda=0.154$ nm, we found corresponding $2\theta=26.93°$ which is the most intense XRD peak as shown in the Figure S1 b corresponds to (012) facet.

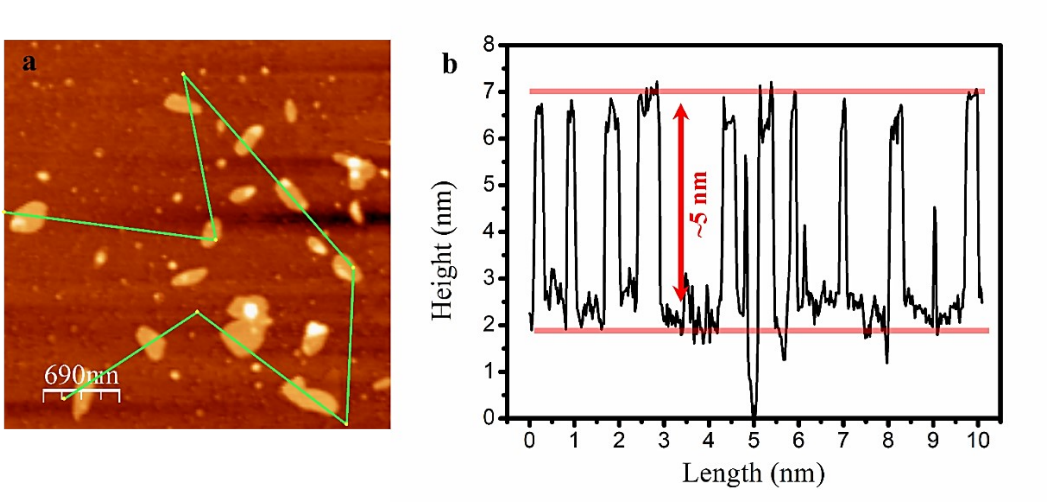

Figure S5: a) AFM image of Bi Flakes, b) line profile to show uniform height profile

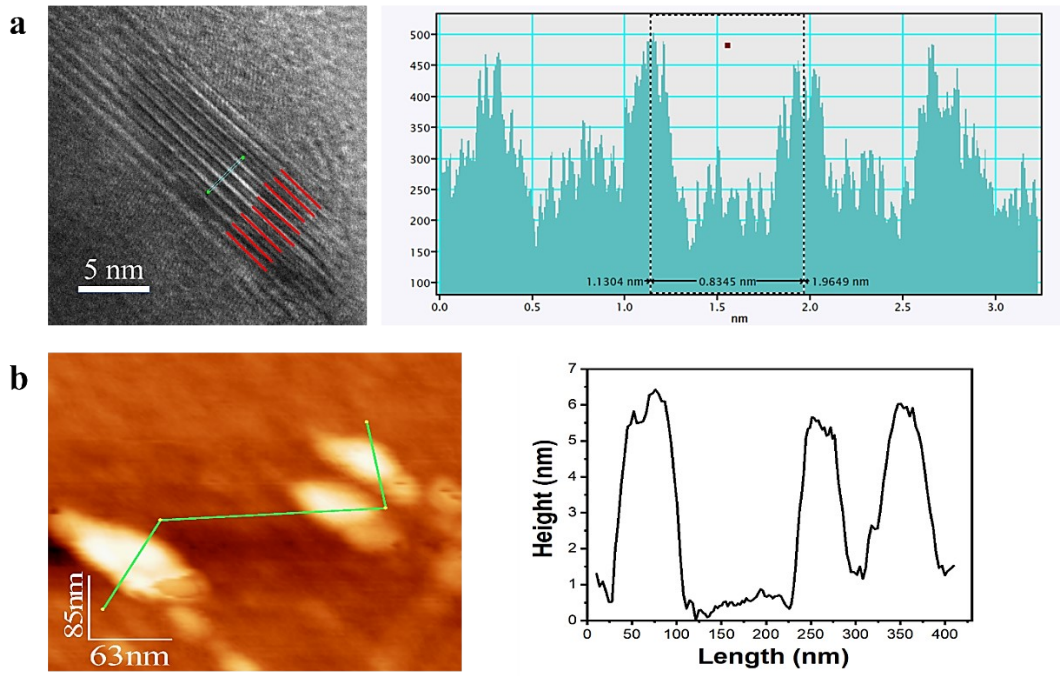

Figure S6: a) Bi flake thickness analysis from HR-TEM of Bi flake cross-section, b) BiOCl AFM image and corresponding line profile

Supplementary Note for Figure S6:

Figure S 6a line profile is shown in the right-side panel. The average distance between two lines is 0.8345 nm and there are eight such lines so the height of the particle will be 7×0.8345 nm=5.8415 nm which is consistent with our AFM data.

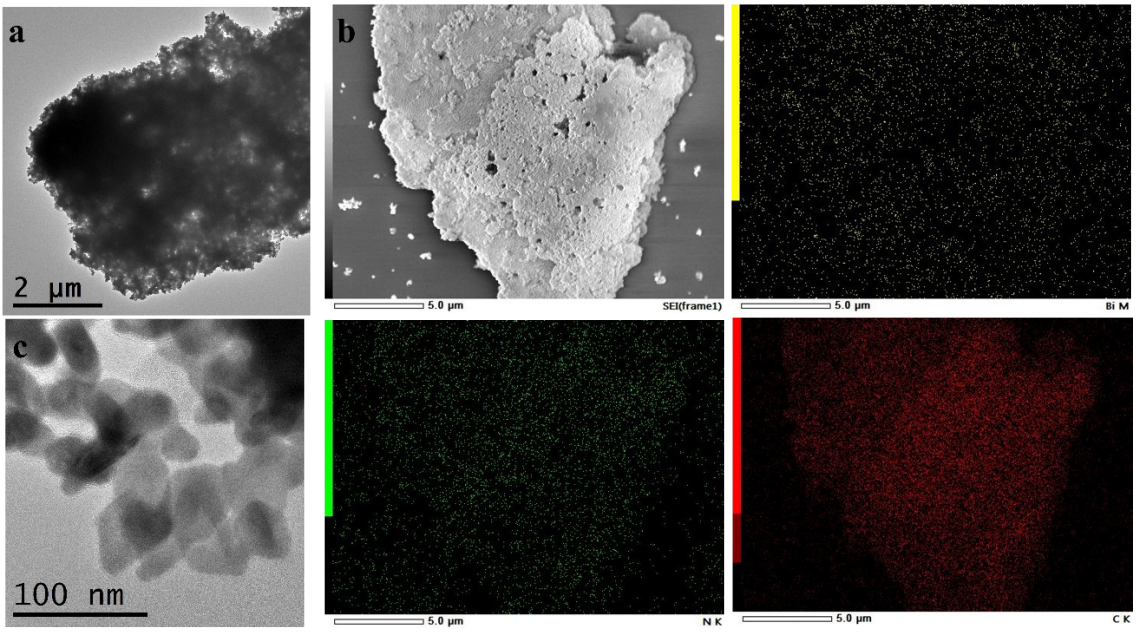

Figure S7: a) FEG-TEM in zoom-out view of P-Bi, b) FE-SEM of P-Bi and corresponding elemental mapping, c) HR-TEM image of P-Bi

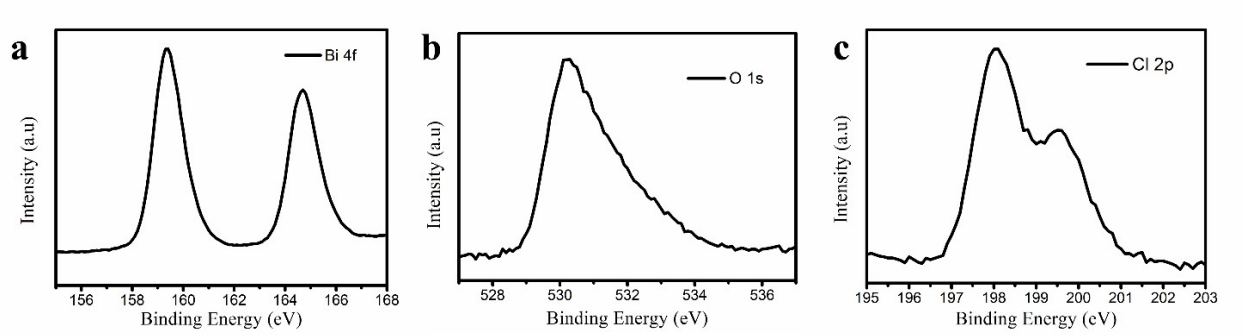

Figure S8: XPS scan of a) Bi 4f, b) O 1s, c) Cl 2p for BiOCl Flakes

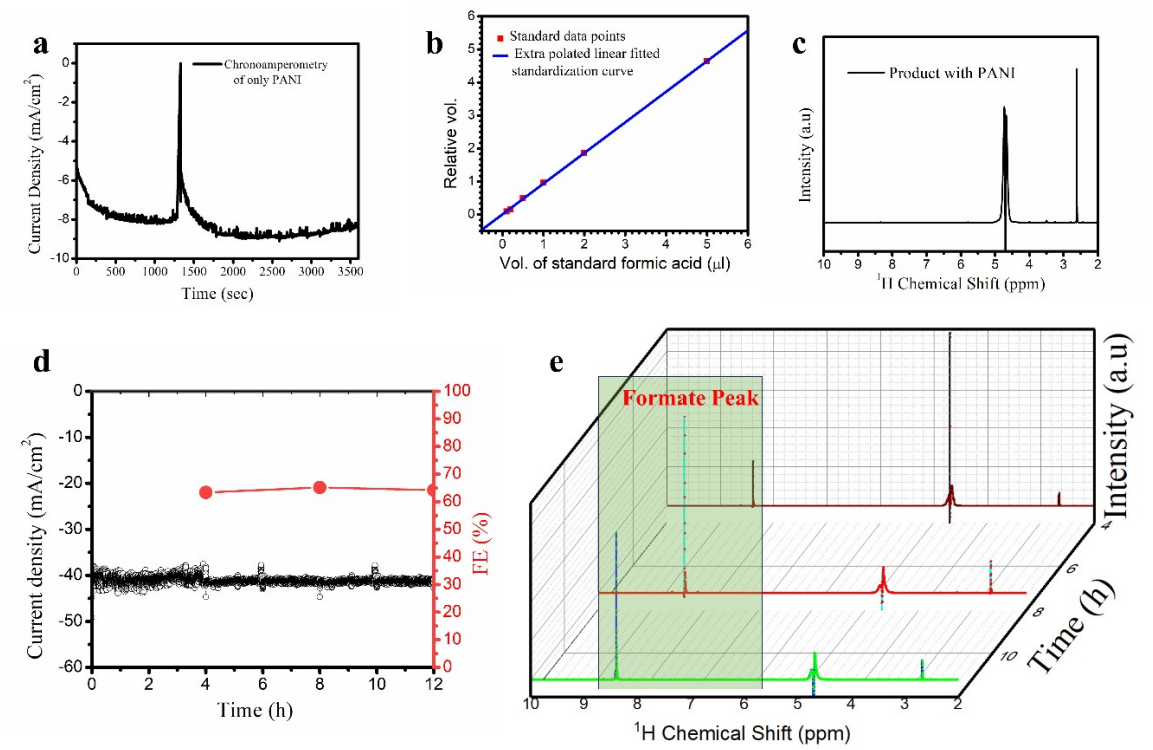

Figure S9: a) chronoamperometry of PANI with a few sec pause, b) Calibration Curve, c) NMR of 1h CA electrolyte with PANI electrode, d) long term stability test at -1.04 V_{RHE}, e) NMR data of corresponding long-term stability test

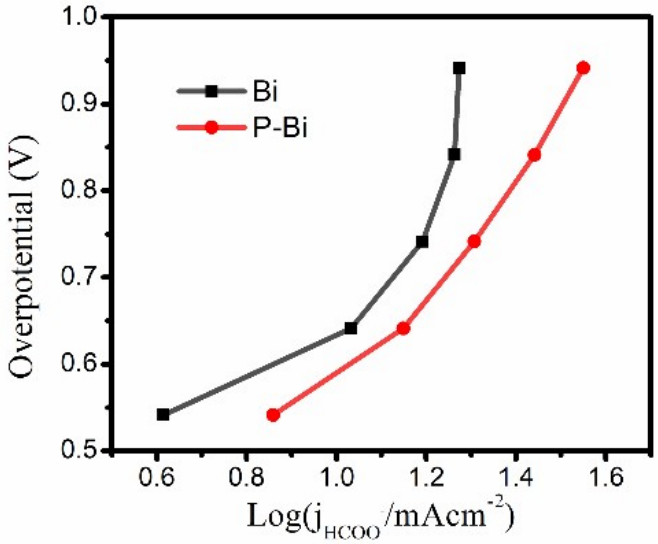

Figure S10: Tafel plot

Supplementary Note for Figure S10:

In figure a, we could not complete the Tafel plot because, at a very low current density, the formate yield is too less to determine the FE with reasonable error. However, from the trend line, we can conclude that the red curve (P-Bi) should have a lesser slope at >0.1V overpotential because at a much lower overpotential region both the curve will tend to converge. This means P-Bi faces less charge transfer resistance than bare Bi flakes.

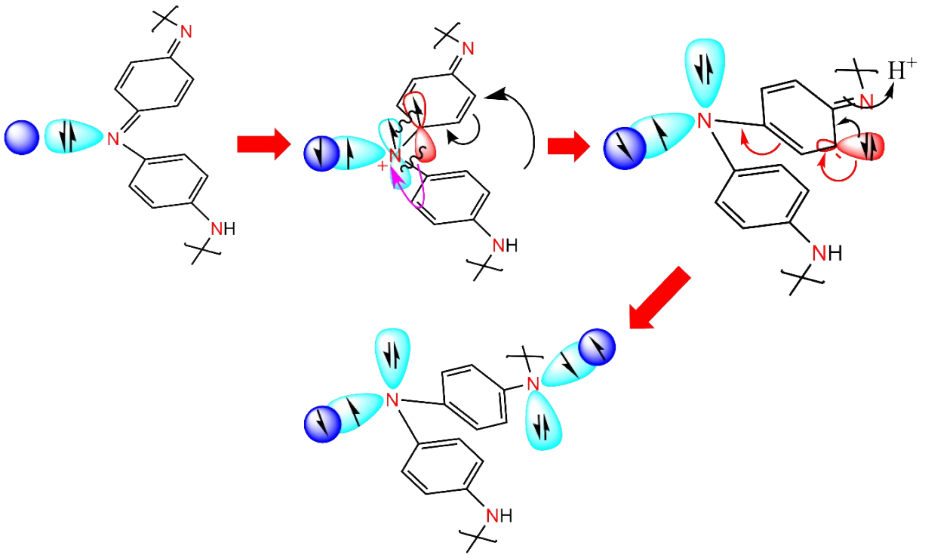

Figure S11: Possible mechanism of PANI reduction under reductive potential

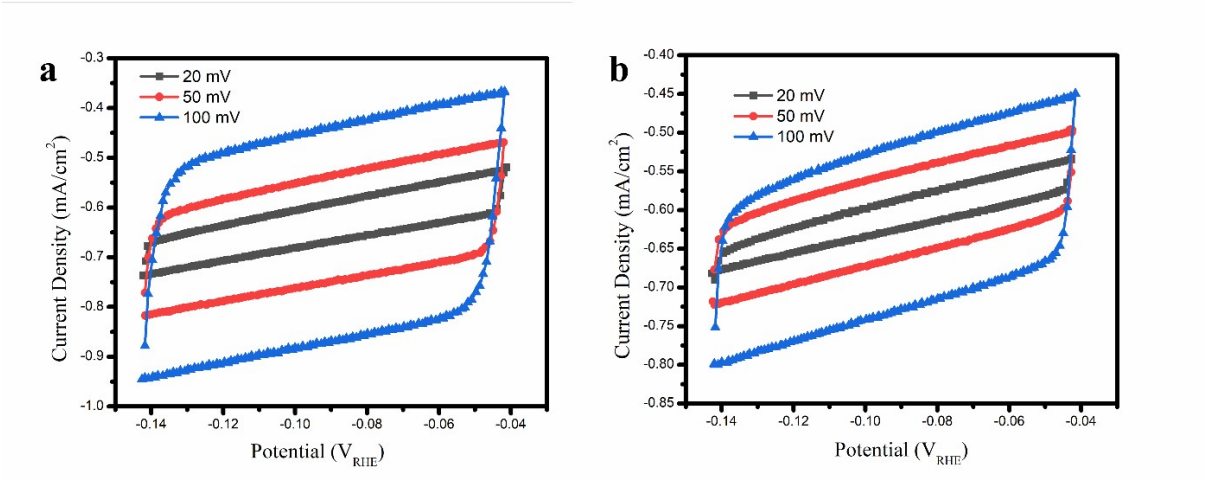

Figure S12: Cyclic Voltammetry Curve for ECSA calculation of a) Bi and b) P-Bi

Supplementary Note for Figure S12:

We found electrochemical double layer capacitance of Bi and P-Bi are 2.22 mF/cm^2 and 1.14 mF/cm^2, respectively. This infers that Bi has more electrochemical surface area (ECSA) than P-Bi. Therefore, we can conclude, higher activity of P-Bi is coming due more active reaction sites, although having lesser ECSA.

Table S1: Comparison of the electrochemical CO_2RR performance

Catalyst	electrolyte	Potential	$j_{formate}$ (mA/cm^2)	Ref
PANI modified Bi flakes (P-Bi)	0.5 M $KHCO_3$	-1.14 V_{RHE}	35.5	This work
Bi flakes	0.5 M $KHCO_3$	-1.14 V_{RHE}	18.7	This work
Nano Bi	0.5 M $KHCO_3$	-1.6 V_{SCE}	9.7	[10]
Bismuthene	0.5 M $KHCO_3$	-0.98 V_{RHE}	42.36	[11]
Bi Nanodendrite	0.5 M $NaHCO_3$	-1.8 V_{SCE}	15.2	[12]
$Bi_2O_2CO_3$	0.5 M $NaHCO_3$	-1 V_{RHE}	24	[13]
BiO_x/C	0.5 M $NaHCO_3$/0.5 M $NaClO_4$	-1.75 $V_{Ag/AgCl}$	16.1	[14]
Bi Nanosheets	0.1 M $KHCO_3$	-1.1 V_{RHE}	14.19 (calculated)	[15]
Bi_2O_3@MCCM	0.1 M $KHCO_3$	-1.26 V_{RHE}	16	[16]
Bi Nanosheets	0.5 M $KHCO_3$	-1.18 V_{RHE}	45	[17]
Mesoporous Bi NS	0.5 M $NaHCO_3$	-1 V_{RHE}	> 17	[18]

References:

1 L. Li, M. Zhang, Z. Zhao, B. Sun and X. Zhang, *Dalt. Trans.*, 2016, **45**, 9497–9505.

2 X. Wang, W.-J. Yin, Y. Si, X. Wang, X. Guo, W. Guo and Y. Fu, *J. Mater. Chem. A*, 2020, **8**, 19938–19945.

3 K. Trentelman, *J. Raman Spectrosc.*, 2009, **40**, 585–589.

4 J. A. Steele and R. A. Lewis, *Opt. Mater. Express*, 2014, **4**, 2133.

5 F. Usman, J. O. Dennis, K. C. Seong, A. Yousif Ahmed, F. Meriaudeau, O. B. Ayodele, A. R. Tobi, A. A. S. Rabih and A. Yar, *Results Phys.*, 2019, **15**, 102690.

6 B. Butoi, A. Groza, P. Dinca, A. Balan and V. Barna, *Polymers (Basel).*, , DOI:10.3390/polym9120732.

7 Z. Tong, Y. Yang, J. Wang, J. Zhao, B.-L. Su and Y. Li, *J. Mater. Chem. A*, 2014, **2**, 4642–4651.

8 B. Mu, J. Tang, L. Zhang and A. Wang, *Sci. Rep.*, 2017, **7**, 5347.

9 S. Palaniappan and B. H. Narayana, *Polym. Adv. Technol.*, 1994, **5**, 225–230.

10 Y. Qiu, J. Du, W. Dong, C. Dai and C. Tao, *J. CO2 Util.*, 2017, **20**, 328–335.

11 C. Cao, D. D. Ma, J. F. Gu, X. Xie, G. Zeng, X. Li, S. G. Han, Q. L. Zhu, X. T. Wu and Q. Xu, *Angew. Chemie - Int. Ed.*, 2020, **59**, 15014–15020.

12 H. Zhong, Y. Qiu, T. Zhang, X. Li, H. Zhang and X. Chen, *J. Mater. Chem. A*, 2016, **4**, 13746–13753.

13 Y. Zhang, X. Zhang, Y. Ling, F. Li, A. M. Bond and J. Zhang, *Angew. Chemie - Int. Ed.*, 2018, **57**, 13283–13287.

14 C. W. Lee, J. S. Hong, K. D. Yang, K. Jin, J. H. Lee, H. Y. Ahn, H. Seo, N. E. Sung and K. T. Nam, *ACS Catal.*, 2018, **8**, 931–937.

15 W. Zhang, Y. Hu, L. Ma, G. Zhu, P. Zhao, X. Xue, R. Chen, S. Yang, J. Ma, J. Liu and Z. Jin, *Nano Energy*, 2018, **53**, 808–816.

16 S. Liu, X. F. Lu, J. Xiao, X. Wang and X. W. Lou, *Angew. Chemie - Int. Ed.*, 2019, **58**, 13828–13833.

17 C. Peng, X. Wu, G. Zeng and Q. Zhu, *Chem. – An Asian J.*, 2021, **16**, 1539–1544.

18 H. Yang, N. Han, J. Deng, J. Wu, Y. Wang, Y. Hu, P. Ding, Y. Li, Y. Li and J. Lu, *Adv. Energy Mater.*, 2018, **8**, 1–6.